

Training-Free Coverless Multi-Image Steganography with Access Control

Minyeol Bae¹ Si-Hyeon Lee¹

Abstract

Coverless Image Steganography (CIS) hides information without explicitly modifying a cover image, providing strong imperceptibility and inherent robustness to steganalysis. However, existing CIS methods largely lack robust access control, making it difficult to selectively reveal different hidden contents to different authorized users. Such access control is critical for scalable and privacy-sensitive information hiding in multi-user settings. We propose MIDAS, a training-free diffusion-based CIS framework that enables multi-image hiding with user-specific access control via latent-level fusion. MIDAS introduces a Random Basis mechanism to suppress residual structural information and a Latent Vector Fusion module that reshapes aggregated latents to align with the diffusion process. Experimental results demonstrate that MIDAS consistently outperforms existing training-free CIS baselines in access control functionality, stego image quality and diversity, robustness to noise, and resistance to steganalysis, establishing a practical and scalable approach to access-controlled coverless steganography.

1. Introduction

In the era of pervasive internet connectivity and AI-generated content (AIGC), data privacy and security have become increasingly important concerns (Yu et al., 2023). Image steganography is a widely used technique for secure communication, where secret information is embedded into visually natural images in a perceptually imperceptible manner, such that only authorized users possessing the secret key or extraction mechanism can recover the hidden content (Simmons, 1984). Image steganography has been applied to a wide range of scenarios, including social media platforms (Gurunath et al., 2021), edge computing (Issac et al., 2025), quantum computing (Bharatwaj & Hasabnis, 2024), and

¹School of Electrical Engineering, Korea Advanced Institute of Science and Technology (KAIST), Daejeon 34141, South Korea. Correspondence to: Si-Hyeon Lee <sihyeon@kaist.ac.kr>.

Preprint.

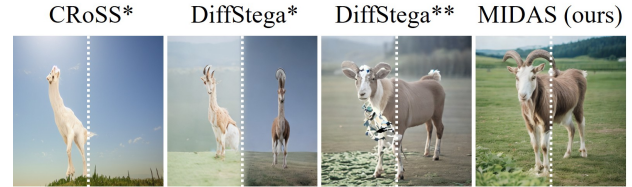


Figure 1. Comparison of stego image quality across training-free CIS methods with two hidden secret images. CRoSS*, DiffStega*, and DiffStega** are extensions of CRoSS and DiffStega based on latent concatenation (see Section 4.1 and Appendix B.2 for details). Dashed lines indicate concatenation boundaries. While baseline methods often suffer from visual artifacts or discontinuities due to limited diversity, MIDAS preserves high visual fidelity and natural image synthesis.

efficient image compression (Jafari et al., 2013).

Traditional image steganography assumes a natural image, referred to as a cover image, and focuses on embedding bit-level messages by modifying the cover at the pixel or transform level (Chan & Cheng, 2004; Mali et al., 2012; Liao et al., 2018), yielding a modified image referred to as a stego image. These approaches are collectively known as modification-based methods. More recently, this modification-based paradigm has been extended to scenarios where secret images are embedded into a cover image (Baluja, 2017). To improve both reconstruction quality and embedding capacity, a growing body of work has leveraged advanced deep neural architectures (Jing et al., 2021; Lu et al., 2021; Guan et al., 2022; Xu et al., 2022).

In multi-image hiding scenarios, multiple secret images are embedded into a single cover image to improve transmission efficiency. In practice, each secret image may be intended for a different receiver, which necessitates access control functionality where only authorized users can recover their designated secrets. Such access control is indispensable in the private sector for managing sensitive databases and protecting industrial secrets, as well as in organizations with differentiated security requirements, including government, military, and diplomatic sectors (Akl & Taylor, 1983). Recent works have explored modification-based approaches to enable access control in multi-image steganography (Kweon et al., 2021; Zhou et al., 2025a;b). However, it is well known that such modification-based methods render the resulting stego image vulnerable to steganalysis, particularly when the original cover image is leaked or predictable, thereby

Table 1. Comparison of image steganography methods.

Method	Coverless	Training	Multi-image	Access control
Baluja		moderate	✓	
HiNet		moderate		
ISN		moderate	✓	
DeepMIH		moderate	✓	
RIIS		moderate	✓	
Kweon et al.		moderate	✓	✓
IIS		moderate	✓	✓
AIS		moderate	✓	✓
CRoSS	✓	free		
DiffStega	✓	free		
DStyleStego	✓	free		
HIS	✓	moderate	✓	
Qin et al.	✓	heavy	✓	
Chen et al.	✓	heavy		
MIDAS(Ours)	✓	free	✓	✓

undermining the fundamental security of the hidden data.

Meanwhile, coverless image steganography (CIS) has emerged as an alternative paradigm that avoids modifying a cover image, often leveraging generative models, thereby achieving strong robustness against steganalysis. Representative CIS methods, such as CRoSS (Yu et al., 2023) and DiffStega (Yang et al., 2024), are particularly appealing because they are training-free, which is crucial for real-world applications given the high computational cost and data requirements associated with training generative models. Furthermore, training-based schemes typically require distributing the entire trained model, which effectively acts as an impractically long secret key. In contrast, training-free schemes rely on publicly available models, enabling significantly more practical and efficient deployment. However, existing training-free CIS methods still suffer from two key limitations:

(1) **Absence of Multi-Image Hiding and Access Control:** Access control functionality inherently requires reliable and effective multi-image hiding; however, existing training-free CIS methods are primarily designed for single-image concealment, and naive extensions to multi-image hiding lead to severe performance degradation.

(2) **Limited Stego Image Diversity:** The generated stego images often preserve substantial residual structural information (Chen et al., 2025). This limitation is particularly pronounced in naive concatenation-based extensions for access control scenarios (see Fig. 1).

Several recent works (Chen et al., 2025; Qin et al., 2025; Xu et al., 2024; Guo et al., 2026) have attempted to address these issues; however, they either require training or rely on the transmission of side information associated with the secret image (see Section 2.1.2 for details). As a

result, a training-free CIS framework with access control capability that does not require transmitting any additional secret-related information is still lacking.

To address this gap, we introduce a novel training-free CIS framework that supports access-controlled multi-image hiding without transmitting any auxiliary information related to the secret images. The main contributions of this work are summarized as follows:

- We propose **MIDAS (Multi-Image Diffusion-based Access-controlled Steganography)**, a novel training-free CIS framework that enables access-controlled multi-image hiding by effectively leveraging pre-trained diffusion models.
- We introduce a Latent Vector Fusion module and a key mechanism termed Random Basis. The Random Basis mechanism neutralizes the inherent structure of noisy latent representations, while the Latent Vector Fusion module reshapes them into representations that are more amenable to the diffusion process. Together, these components significantly improve both the perceptual quality and diversity of the generated stego images (see Fig. 1).
- Through extensive experiments, we demonstrate that MIDAS consistently outperforms existing training-free CIS baselines in terms of access control functionality, stego image quality and diversity, robustness to noise, and resistance to steganalysis.

Table 1 summarizes the distinguishing features of our work in comparison with existing studies, and Section 2.1 presents a more detailed review of the related literature.¹

2. Related Work and System Model

2.1. Related Work

2.1.1. COVER-BASED IMAGE STEGANOGRAPHY

The paradigm of hiding secret images within other images has gained widespread interest, a concept first introduced by Baluja (2017) using deep neural networks. Building on this foundation, several studies have adopted Invertible Neural Networks (INNs) to improve reconstruction quality, including HiNet (Jing et al., 2021), ISN (Lu et al., 2021), DeepMIH (Guan et al., 2022), and RIIS (Xu et al., 2022).

Despite these advancements, achieving access-controlled multi-image hiding remains a significant challenge; incorporating user-selective private keys often requires additional metadata that can degrade the quality of both stego and

¹The source code of the proposed algorithm is available in the supplementary material.

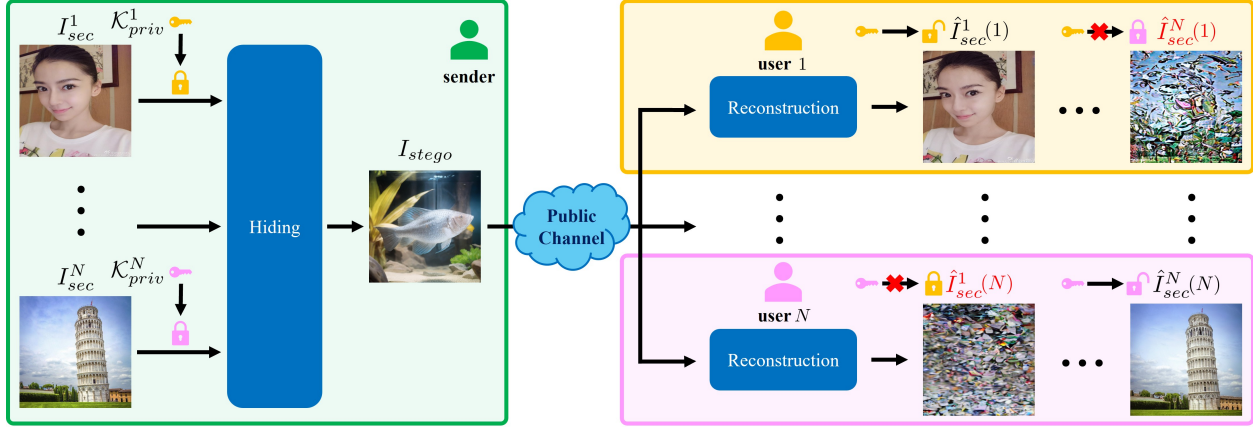


Figure 2. The overall scenario. The sender embeds multiple secret images ($I_{sec}^1, \dots, I_{sec}^N$) into a single stego image (I_{stego}), which is then transmitted through a public channel. Each secret image I_{sec}^i is encrypted with a private key \mathcal{K}_{priv}^i . Let $\hat{I}_{sec}^j(i)$ denote the reconstruction result of secret image j obtained by user i using \mathcal{K}_{priv}^i . Due to the access control function, only the intended receiver i possessing \mathcal{K}_{priv}^i can successfully recover $\hat{I}_{sec}^i(i)$, whereas for any other image $j \neq i$, the reconstruction $\hat{I}_{sec}^j(i)$ results in a meaningless output.

reconstructed images (Zhou et al., 2025b). Kweon et al. (2021) integrate the private keys into multi-image steganography, providing a foundation for access control. Following this, IIS (Zhou et al., 2025a) and AIS (Zhou et al., 2025b) employ INN-based architectures to further enhance reconstruction quality and capacity. Nevertheless, these methods are modification-based and thus inherently vulnerable to steganalysis. In contrast, MIDAS achieves access control in a coverless manner, thereby fundamentally enhancing security by eliminating the need for cover image modification.

2.1.2. COVERLESS IMAGE STEGANOGRAPHY

CIS is fundamentally robust against steganalysis as it avoids cover image modification. Many CIS schemes utilize generative models to synthesize stego images directly from secret images. However, optimizing high-quality generators is a resource-intensive process. In this regard, training-free approaches offer significant advantages. CRoSS (Yu et al., 2023) utilizes the Denoising Diffusion Implicit Model (DDIM) (Song et al., 2021) inversion process to hide data in two stages: a secret image is first mapped to a noisy latent using a private prompt (private key), then transformed into a stego image via the backward process guided by a public prompt (public key). The secret image is subsequently retrieved by exploiting the inherent reversibility of DDIM. Note that CRoSS faces notable challenges: it relies on secret image-dependent private prompts that must be transmitted for each session, and its limited editing capabilities often leave residual structural information in the stego image, thereby hindering naive extensions to multi-image hiding. DiffStega (Yang et al., 2024) eliminates the need for private prompts by replacing them with a fixed null-text prompt and applying a private key mechanism directly to noisy latents. While it improves stego image quality by integrating a reference image and ControlNet (Zhang et al., 2023), its

editing capability remains restricted. DStyleStego (Guo et al., 2026) improves editing performance, but it requires the transmission of information related to the secret image and remains restricted to single-image hiding. Consequently, these training-free methods are either not readily extendable to multi-image hiding or require the transmission of secret-related information.

Some recent CIS methods have attempted to overcome the aforementioned limitations through specialized training. For instance, Chen et al. (2025) and Qin et al. (2025) employ steganography-specific generators to enhance editing capabilities, with the latter further enabling multi-image hiding scenarios. However, these methods entail substantial computational overhead due to their reliance on high-quality generator training. Another approach, HIS (Xu et al., 2024), generates a stego image via CRoSS to serve as a cover for subsequent modification-based steganography to enable multi-image hiding, while still necessitating the transmission of additional information related to secret images for every communication. Furthermore, none of the aforementioned approaches provide an explicit access control function. In contrast, MIDAS enables access-controlled CIS even within a training-free framework without requiring the transmission of secret-related information, thereby offering a practical and secure solution for real-world scenarios.

2.2. System Model

We consider a multi-image access-controlled steganography scenario with a single sender and N receivers (users), as illustrated in Fig. 2. The sender possesses N secret images ($I_{sec}^1, \dots, I_{sec}^N$) and N private keys ($\mathcal{K}_{priv}^1, \dots, \mathcal{K}_{priv}^N$), and the i -th receiver has the private key \mathcal{K}_{priv}^i . We further allow for the existence of certain public resources shared between the sender and the receivers. Under a strong attacker model,

these public resources are assumed to be fully accessible to the attacker as well. All the secret images are jointly embedded into a single stego image I_{stego} using the private keys and the public resources, which is transmitted over a public channel. The resulting stego image is required to be visually indistinguishable from a natural image. Upon receiving I_{stego} , each receiver attempts to reconstruct the embedded secret images. The i -th receiver, who possesses only the private key \mathcal{K}_{priv}^i , is required to obtain a faithful reconstruction $\hat{I}_{sec}^i(i)$ of its designated secret image I_{sec}^i . In contrast, for any other image $j \neq i$, the reconstructed output $\hat{I}_{sec}^j(i)$ by the i -th receiver should reveal no useful information about I_{sec}^j .

3. Method

3.1. Overview

This section introduces MIDAS, a novel access-controlled image steganography method utilizing a diffusion model. For both Hiding and Reconstruction Stages, MIDAS employs a latent diffusion model (Rombach et al., 2022) with a DDIM sampler (Song et al., 2021). The inherent inversion property of DDIM is utilized to enable the reconstruction of secret images. In addition, it integrates EDICT (Wallace et al., 2023), an exact inversion method, to further improve the reconstruction quality. In MIDAS, private keys are given as random seeds. The public resources consist of a public key \mathcal{K}_{pub} corresponding to an additional random seed and a public prompt \mathcal{P}_{pub} , which together facilitate the generation of stego images. The model operates in a latent space with $C \times H \times W$ dimensions, where C denotes the channel dimension and H and W are the spatial dimensions of the latent representation. The Hiding and Reconstruction Stages of MIDAS are illustrated in Fig. 5 of Appendix A, and are described in Sections 3.2 and 3.3, respectively.

In MIDAS, a Reference Generator (RefGen), utilizing \mathcal{K}_{pub} and \mathcal{P}_{pub} , generates a reference image I_{ref} . I_{ref} is essential for enhancing the visual quality of I_{stego} . Since I_{ref} is generated deterministically from public resources (\mathcal{K}_{pub} and \mathcal{P}_{pub}), it does not need to be explicitly transmitted. The detailed operation and architecture of RefGen are discussed in Section 3.4.

3.2. Hiding Stage

In this stage, N secret images ($I_{sec}^1, \dots, I_{sec}^N$) are first individually encrypted using their corresponding private keys ($\mathcal{K}_{priv}^1, \dots, \mathcal{K}_{priv}^N$). The resulting encrypted data are then jointly processed and fused to a single stego image (I_{stego}). This stage consists of the following steps.

Forward Diffusion. Each secret image I_{sec}^i is first downsampled and mapped to a noisy latent representation $\mathbf{z}_{sec}^i \in$

$\mathbb{R}^{C \times \frac{H}{N_1} \times \frac{W}{N_2}}$ using a forward diffusion module, guided by a null-text prompt. The downsampling factors, N_1 and N_2 (where $N_1 N_2 = N$), are strategically chosen to ensure that the concatenated latent vector of all N secret images precisely matches the base latent dimension of the diffusion model, $\mathbb{R}^{C \times H \times W}$, e.g., $N_1 = 2$ and $N_2 = 1$ when $N = 2$, and $N_1 = N_2 = 2$ when $N = 4$.

Private Key Encryption. For user access control, each \mathbf{z}_{sec}^i is encrypted into $\mathbf{z}_{prot}^i \in \mathbb{R}^{C \times \frac{H}{N_1} \times \frac{W}{N_2}}$ using the private key \mathcal{K}_{priv}^i . For any d -dimensional input vector \mathbf{z} , we consider an encryption strategy that can be expressed in the following form:

$$\mathbf{z}_{enc} = M_d \mathbf{z}, \quad (1)$$

where $\mathbf{z}_{enc} \in \mathbb{R}^d$ is the encrypted latent vector, $\mathbf{z} \in \mathbb{R}^d$ is the vector to be encrypted, and $M_d \in \mathbb{R}^{d \times d}$ is an orthonormal matrix chosen by the encryption strategy. Due to the orthonormal property of M_d , the original vector can be perfectly reconstructed as $\mathbf{z} = M_d^T \mathbf{z}_{enc}$, where M_d^T denotes the transpose of M_d . The previously suggested Noise Flip (Yang et al., 2024) mechanism, which flips the signs of the elements of the input vector, used $M_d = \text{diag}(e)$ with $e \in \{-1, 1\}^d$.

We employ a Random Basis mechanism, which constructs $M_d = Q_d(\mathcal{K}, \gamma)$, where $Q_d(\mathcal{K}, \gamma)$ is an orthonormal matrix generated from the seed \mathcal{K} and the strength γ . The hyperparameter γ determines the proportion of \mathbf{z} 's elements that are affected by the transformation Q_d , i.e., γ portion of \mathbf{z} 's elements are transformed by Q_d while the remaining elements are left identical. Further details regarding the construction of Q_d can be found in Appendix B.1.

By applying the Random Basis to \mathbf{z}_{sec}^i with the private key \mathcal{K}_{priv}^i and strength γ_{priv} , we have $\mathbf{z}_{prot}^i = Q_d(\mathcal{K}_{priv}^i, \gamma_{priv}) \mathbf{z}_{sec}^i$. Despite its conceptual simplicity, the Random Basis empirically demonstrates superior performance compared to Noise Flip; further details are provided in Appendix D.1.

Latent Vector Fusion. To enable multi-image hiding within a single transmission, the sender concatenates all \mathbf{z}_{prot}^i vectors to form a combined latent vector, denoted as $\mathbf{z}_{prot} \in \mathbb{R}^{C \times H \times W}$. However, simple concatenation results in a stego image with abrupt and visible boundaries at the concatenated interfaces (see Fig. 1). This phenomenon occurs because residual information of the original secret images remains within the noisy latent representations (\mathbf{z}_{prot}^i) even after the DDIM forward process (Greenberg et al., 2025). Consequently, the backward diffusion model struggles to smoothly blend these structurally distinct latent segments. This results in a stego image that is visibly fragmented along the concatenation seam, rendering the output image unnatural and unsuitable for steganography.

To mitigate this, a Latent Vector Fusion step utilizing the

public key \mathcal{K}_{pub} is applied. This process shuffles the concatenated latent vector \mathbf{z}_{prot} and incorporates some reference component, thereby ensuring the generation of a visually high-quality stego image. The Latent Vector Fusion process is defined as:

$$\mathbf{z}_{pub} = \sqrt{\alpha}M_D\mathbf{z}_{prot} + \sqrt{1 - \alpha}\mathbf{z}_{ref}. \quad (2)$$

Here, $\mathbf{z}_{pub} \in \mathbb{R}^{C \times H \times W}$ is the resulting latent vector, \mathbf{z}_{prot} is the concatenated vector. $M_D = Q_D(\mathcal{K}_{pub}, \gamma_{fuse}) \in \mathbb{R}^{D \times D}$ is constructed via the Random Basis mechanism with input dimension $D = C \times H \times W$, public key \mathcal{K}_{pub} , and strength γ_{fuse} . This transformation serves to mix the spatial components of \mathbf{z}_{prot} , thereby removing the localized spatial information caused by the concatenation. $\mathbf{z}_{ref} \in \mathbb{R}^{C \times H \times W}$ is the noisy latent vector of the reference image I_{ref} , used to further enhance the stego image generation quality. α is a mixing coefficient that controls the proportions of the transformed vector component ($M_D\mathbf{z}_{prot}$) and \mathbf{z}_{ref} .

Reverse Diffusion. The stego image I_{stego} is generated by applying the reverse diffusion process to \mathbf{z}_{pub} conditioned on the public prompt \mathcal{P}_{pub} and the reference image I_{ref} . I_{stego} is then transmitted through the public channel.

3.3. Reconstruction Stage

In this stage, each user reconstructs their corresponding secret image. Crucially, this stage verifies the user’s identity using their private key, thereby ensuring that only the intended recipient can correctly decode their assigned secret image from I_{stego} . Since I_{stego} may be damaged during transmission, each user receives \tilde{I}_{stego} , a potentially degraded version of I_{stego} . This stage proceeds through the following steps.

Forward Diffusion. Using DDIM inversion, the received image \tilde{I}_{stego} is inverted to infer $\tilde{\mathbf{z}}_{pub} \in \mathbb{R}^{C \times H \times W}$, an approximation of \mathbf{z}_{pub} . \mathcal{P}_{pub} and I_{ref} are used as conditions for this DDIM inversion.

Latent Vector Decomposition. In this step, each user performs the inverse operation of the Latent Vector Fusion. From $\tilde{\mathbf{z}}_{pub}$, the user first remove the \mathbf{z}_{ref} component and then apply the inverse Random Basis transformation to obtain $\hat{\mathbf{z}}_{prot} \in \mathbb{R}^{C \times H \times W}$. This decomposition process is represented by the following equation:

$$\hat{\mathbf{z}}_{prot} = M_D^T \left(\frac{\tilde{\mathbf{z}}_{pub} - \beta\mathbf{z}_{ref}}{\alpha} \right) \quad (3)$$

User Access Control. The vector $\hat{\mathbf{z}}_{prot}$ consists of N segments, where the i -th segment corresponds to I_{sec}^i . User i attempts to decrypt all N segments using its private key \mathcal{K}_{priv}^i , yielding $\hat{\mathbf{z}}_{sec}(i) \in \mathbb{R}^{C \times H \times W}$. Crucially, since only the i -th segment was originally protected by \mathcal{K}_{priv}^i , only this segment’s decryption yields a meaningful latent representa-

tion. This difference in decryption quality across segments implements the access control function.

Backward Diffusion and Image Reconstruction. We utilize a joint denoising approach on the full vector $\hat{\mathbf{z}}_{sec}(i)$ through the DDIM backward process, conditioned on the null-text prompt. The resulting vector is then segmented. This method demonstrates superior performance compared to segmenting first and then applying the DDIM backward process to each segment. The detailed description of this diffusion policy is discussed in Appendix D.2.

The correctly decrypted i -th segment, $\hat{\mathbf{z}}_{sec}^i(i) \in \mathbb{R}^{C \times \frac{H}{N_1} \times \frac{W}{N_2}}$ serves as an approximation of the true secret latent vector \mathbf{z}_{sec}^i . This $\hat{\mathbf{z}}_{sec}^i(i)$ is passed into the VAE decoder and upsampling block to obtain the final reconstructed image, $\hat{I}_{sec}^i(i)$. If user i attempts to reveal another user’s image using the non-decrypted segment $\hat{\mathbf{z}}_{sec}^j(i) \in \mathbb{R}^{C \times \frac{H}{N_1} \times \frac{W}{N_2}}$ ($j \neq i$), the resulting image $\hat{I}_{sec}^j(i)$ will exhibit significant degradation, as $\hat{\mathbf{z}}_{sec}^j(i)$ significantly deviates from the true latent vector \mathbf{z}_{sec}^j .

3.4. Reference Generator

In this subsection, we provide the details of RefGen. RefGen is a pre-trained diffusion model that takes the public resources (\mathcal{K}_{pub} and \mathcal{P}_{pub}) as input to generate the reference image I_{ref} . The process begins by using \mathcal{K}_{pub} to generate the initial Gaussian noise. Since the diffusion process is deterministic when the random seed (here, \mathcal{K}_{pub}) is fixed, the diffusion model always generates the identical image I_{ref} from the same \mathcal{K}_{pub} and \mathcal{P}_{pub} . This deterministic property is critical, as it eliminates the need to explicitly transmit I_{ref} , allowing both the sender and the designated recipient to locally reproduce I_{ref} .

Prior work (Yang et al., 2024) leverages ControlNet (Zhang et al., 2023) to condition the I_{ref} generation using a control image (e.g., the OpenPose bone image or semantic segmentation map) extracted from the secret image. This methodology, however, presents two critical limitations. First, note that the control image must be shared publicly. Thus, publicly transmitting the structural control image compromises the covertness by exposing secret image information. Second, the rigid conditioning significantly restricts the generated image’s diversity and flexibility, often leading to poor quality when the control image and prompt are semantically inconsistent. To address these issues, we deliberately omit the use of control images in MIDAS. Instead, we achieve the high-quality conditional generation required for steganography by incorporating a Random Basis along with a Latent Vector Fusion mechanism. The combination of Random Basis and Latent Vector Fusion allows us to effectively embed the secret information while ensuring high fidelity, thereby eliminating the need for the external, restrictive conditioning

provided by control images.

4. Experiment

4.1. Experimental Settings

Implementation. Consistent with prior work (Yang et al., 2024), we utilize Stable Diffusion v1.5² for both the forward diffusion in the Hiding Stage and backward diffusion in the Reconstruction Stage. PicX_real³ is employed for RefGen. Further details are provided in Appendix B.2.

Datasets. We employ the Stego260 (Yu et al., 2023) and UniStega (Yang et al., 2024) datasets, which are specifically designed for diffusion steganography. These datasets include the images with their text descriptions (source caption) and semantically modified text descriptions (target caption). We only use the target caption for \mathcal{P}_{pub} and a null-text is used for private prompt. These datasets are directly adopted for the $N = 1$ case. To align the dataset with our multi-image hiding scenario (which requires N secret images per stego image), we randomly sample N images as secret images and independently select a single text prompt from the entire set of prompts in the dataset. Unless otherwise specified, all experiments are conducted with $N = 2$.

Metrics. We evaluate image hiding and reconstruction quality using Peak Signal-to-Noise Ratio (PSNR), Structural Similarity Index (SSIM) (Wang et al., 2004), and Learned Perceptual Image Patch Similarity (LPIPS) (Zhang et al., 2018). The CLIP Score (Radford et al., 2021) measures the semantic alignment between I_{stego} and \mathcal{P}_{pub} . In addition, Multi-dimension Attention Network for no-reference Image Quality Assessment (MANIQA) (Yang et al., 2022) is employed to assess the perceived visual naturalness of the generated stego images, reflecting human judgment. All quantitative results are reported as the average over three independent trials with different random seeds.

Baselines. For training-free CIS baselines, we consider CRoSS (Yu et al., 2023) and DiffStega (Yang et al., 2024), detailed in Section 2.1.2. To evaluate the multi-image hiding scenario (i.e., $N > 1$), we adapted CRoSS and DiffStega into CRoSS* and DiffStega*, respectively. For CRoSS*, we utilized source captions as private keys and concatenated the noisy latents of the secret images. DiffStega* was modified by applying Noise Flip with \mathcal{K}_{priv} to each noisy latent before concatenation, followed by an additional Noise Flip with \mathcal{K}_{pub} on the resulting vector. For both CRoSS* and DiffStega*, the public prompt \mathcal{P}_{pub} is employed to generate the stego images. While the original DiffStega utilizes control images, we omit them in DiffStega* for the rea-

sons discussed in Section 3.4. For consistency, the names CRoSS* and DiffStega* are used throughout the paper, even for the $N = 1$ case where they remain functionally identical to the original models. Detailed implementation settings are provided in Appendix B.2.

We maintained the original parameters specified in the baseline studies for both CRoSS* and DiffStega*. In contrast, we also evaluated these baselines using the settings adjusted to MIDAS within our ablation studies (see Appendix D.3). This allowed us to assess the contribution of Latent Vector Fusion, validating their superiority over the conventional approaches even under identical experimental conditions.

For access-controlled image steganography baselines, we consider IIS (Zhou et al., 2025a) and AIS (Zhou et al., 2025b), even though they are modification-based (neither coverless nor training-free) methods.

4.2. Experimental Results

Qualitative Results. Fig. 3 provides a visual comparison among training-free CIS methods. Due to the limited editing capability of CRoSS* and DiffStega*, stego images generated by these methods exhibit noticeable visual fragmentation and degraded quality. Furthermore, when extended to the multi-image scenario, CRoSS* struggles significantly to reconstruct the secret images. While DiffStega* shows relatively better reconstruction with the correct \mathcal{K}_{priv} (e.g., $\hat{I}_{sec}^1(1)$, $\hat{I}_{sec}^2(2)$), it fails to enforce access control, as meaningful reconstructions are still achievable even with incorrect \mathcal{K}_{priv} (e.g., $\hat{I}_{sec}^1(2)$, $\hat{I}_{sec}^2(1)$). In contrast, MIDAS produces high-fidelity stego images and demonstrates robust access control; it provides superior reconstruction quality for authorized users while yielding reconstruction failures when an incorrect \mathcal{K}_{priv} is applied. More results are available in Appendix C.1.

Quantitative Results. Table 2 provides a quantitative comparison of MIDAS against baseline methods on the Stego260 dataset. Additional experimental results conducted on the UniStega dataset are provided in Appendix C.2. We define stego image diversity as the dissimilarity (e.g., low PSNR and SSIM, or high LPIPS) between each secret image and its corresponding region in the stego image, where the layout is partitioned by the concatenation boundaries. The CLIP Score also contributes to stego image diversity assessment, as it reflects the model’s capability for prompt-aligned image generation. High diversity is crucial for security, as it prevents third parties from predicting the secret content. We measure stego image quality using MANIQA, which provides a state-of-the-art assessment of visual naturalness that aligns closely with human perception.

CRoSS* and DiffStega* exhibit poor stego image diversity; their generated stego images remain highly similar to the

²<https://huggingface.co/runwayml/stable-diffusion-v1-5>

³<https://huggingface.co/GraydientPlatformAPI/picx-real>

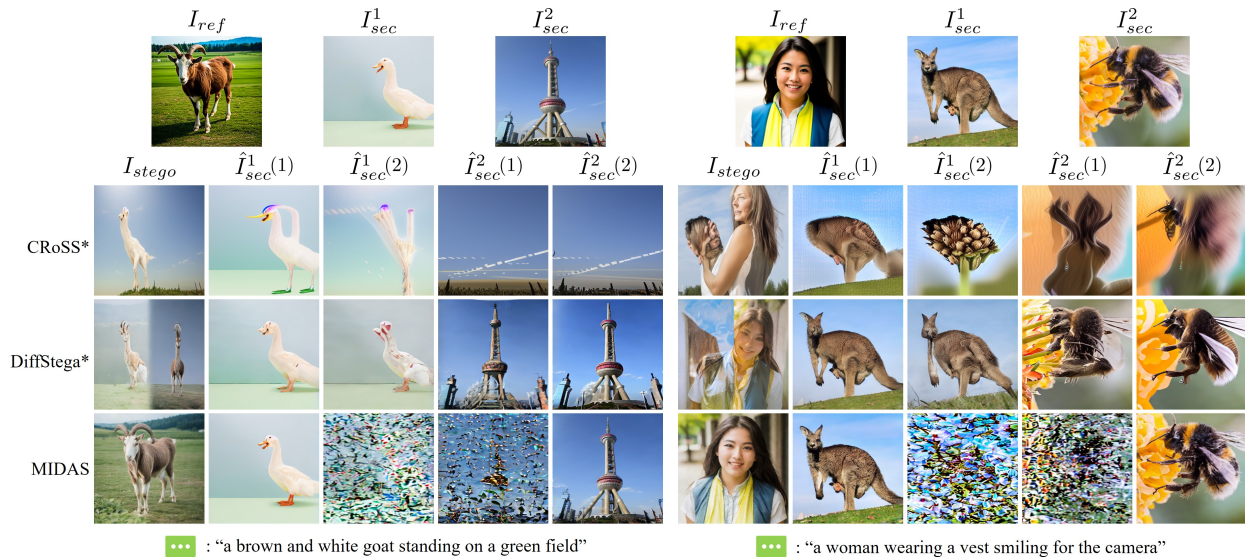


Figure 3. Visual comparisons of MIDAS, CRoSS*, and DiffStega* on the Stego260 dataset under different prompts for two-image hiding.

Table 2. Quantitative results for stego and reconstructed images on the Stego260 dataset.

N	Method	Stego image quality		Stego image diversity			Correct \mathcal{K}_{priv} reconstruction			Wrong \mathcal{K}_{priv} reconstruction		
		MANIQA \uparrow	PSNR \downarrow	SSIM \downarrow	LPIPS \uparrow	CLIP Score \uparrow	PSNR \uparrow	SSIM \uparrow	LPIPS \downarrow	PSNR \downarrow	SSIM \downarrow	LPIPS \uparrow
1	IIS	-	-	-	-	-	48.588	0.999	0.016	10.551	0.107	0.818
	AIS	-	-	-	-	-	35.990	0.999	0.127	22.981	0.595	0.367
	CRoSS*	0.409	20.535	0.740	0.322	27.937	22.870	0.796	0.263	18.387	0.650	0.430
	DiffStega*	0.450	19.686	0.664	0.419	28.871	24.958	0.833	0.232	19.447	0.650	0.397
	MIDAS(Ours)	0.429	13.407	0.419	0.610	29.686	25.161	0.831	0.234	12.718	0.237	0.698
2	IIS	-	-	-	-	-	41.360	0.995	0.070	11.883	0.219	0.808
	AIS	-	-	-	-	-	30.724	0.973	0.317	4.540	0.126	0.847
	CRoSS*	0.406	15.550	0.521	0.579	26.071	17.606	0.563	0.496	15.270	0.470	0.576
	DiffStega*	0.399	17.065	0.531	0.555	26.952	21.908	0.728	0.344	18.137	0.587	0.458
	MIDAS(Ours)	0.434	9.885	0.287	0.752	30.129	23.903	0.771	0.299	9.964	0.090	0.753
4	IIS	-	-	-	-	-	33.540	0.976	0.184	15.783	0.338	0.686
	AIS	-	-	-	-	-	28.045	0.956	0.369	5.131	0.126	0.947
	CRoSS*	0.418	13.445	0.453	0.687	24.601	13.190	0.312	0.681	12.731	0.297	0.696
	DiffStega*	0.364	16.160	0.509	0.600	27.367	19.233	0.609	0.442	17.533	0.545	0.508
	MIDAS(Ours)	0.479	8.996	0.296	0.787	30.169	22.283	0.697	0.359	9.399	0.118	0.763

secret images and fail to align with \mathcal{P}_{pub} (i.e., low CLIP Score). This low diversity not only severely compromises security but also makes concatenation-based multi-image hiding highly challenging, as it often leads to visually fragmented stego image generation in multi-user scenarios. Consequently, the stego image quality of these baseline methods deteriorates significantly as N increases; specifically, DiffStega* suffers from a sharp decline in visual quality (indicated by MANIQA values), while CRoSS* fails to generate images aligned with the prompts (indicated by extremely low CLIP Scores). In contrast, MIDAS exhibits both high stego image quality (high MANIQA) and superior diversity (extremely low similarity with the secret images) regardless of N . This demonstrates the suitability and scalability of MIDAS for multi-image hiding scenarios. Furthermore, evaluations under a larger number of secret images (e.g.,

$N = 8$) are provided in Appendix C.3 to further validate the robustness of our framework in high-capacity settings.

Furthermore, the data confirms the robustness of MIDAS’s access control functionality. Unlike CRoSS* and DiffStega*, where unauthorized reconstruction often remains possible, MIDAS exhibits a significant difference in similarity metrics between the reconstructed image and the secret image when the correct \mathcal{K}_{priv} is used (high similarity) versus when the wrong \mathcal{K}_{priv} is applied (low similarity). This provides quantitative validation that the access control mechanism is successfully implemented, consistent with the qualitative results (Fig. 3).

Although modification-based methods (IIS and AIS) show superior performance compared to training-free CIS methods, they inherently possess security vulnerabilities. More

Table 3. PSNR(dB) of reconstructed images under practical degradations. For Gaussian noise and JPEG compression, standard deviation $\sigma = 5$ and quality factor $Q = 70$ are used, respectively. Considering these degradations as additional noise, 5 additional denoising steps are applied to the diffusion-based frameworks (CRoSS*, DiffStega*, and MIDAS) in the Reconstruction Stage.

Method	Clean	Gaussian noise	JPEG compression
IIS	41.360	12.439	10.047
AIS	30.774	14.654	9.442
CRoSS*	17.606	16.300	16.932
DiffStega*	21.908	20.076	20.422
MIDAS(Ours)	23.903	20.046	19.922

precisely, the resulting modification leaves inevitable traces in the stego image, making it easily detectable if the original cover image is exposed. Furthermore, these methods are training-based, requiring additional optimization overhead.

Anti-Steganalysis. Steganalysis methods aim to distinguish between stego images and cover images. We evaluate the security of MIDAS compared to baseline methods using the state-of-the-art steganalysis methods: XuNet (Xu et al., 2016) and SiaStegNet (You et al., 2021). These models are trained on cover-stego pairs to identify steganographic traces, with their detection accuracy generally improving as the training dataset size increases. Since coverless steganography methods lack of cover images, we utilize images generated from the same model and prompts as the corresponding cover images. Specifically, these cover images are generated using a randomly sampled noise vector under the same \mathcal{P}_{pub} as the stego images. Fig. 4 presents the steganalysis accuracy results across varying training data sizes. Modification-based methods (IIS and AIS) consistently achieve high steganalysis accuracy ($> 90\%$), because the embedding modifications leave inherent traces within the stego images, allowing the steganalysis models to distinguish them from the original covers. Although CRoSS* and DiffStega* are coverless methods, their poor stego image quality introduces visible artifacts, causing its steganalysis accuracy to rapidly converge to a high value ($> 85\%$). In contrast, the steganalysis accuracy of MIDAS is approximately 20% lower than that of other baselines, significantly limiting the detector’s confidence and demonstrating enhanced security. This resilience stems from its coverless approach combined with its superior stego image generation quality, which ensures the stego images remain highly statistically similar to genuinely generated images.

Robustness. We evaluate the robustness against noise introduced during the transmission of the stego image. Table 3 reports the reconstruction quality when the stego image is corrupted by Gaussian noise or compressed using JPEG. Even under strong degradation, MIDAS maintains an acceptable level of secret information transmission. In contrast, existing modification-based access control methods

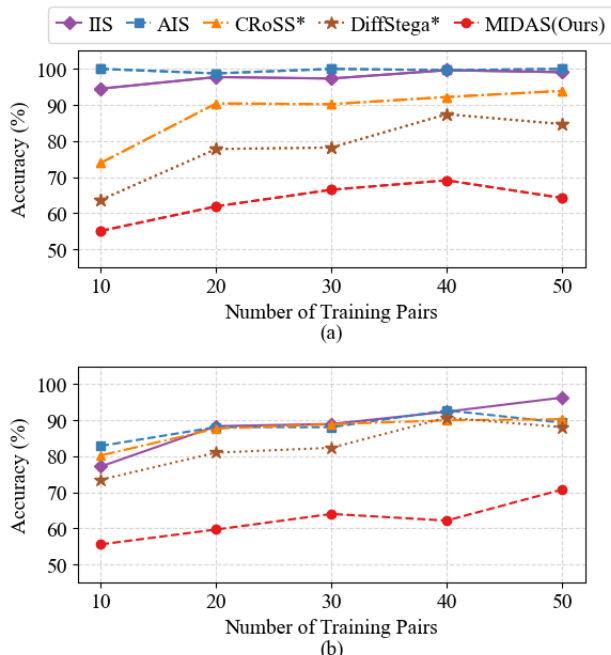


Figure 4. Steganalysis accuracy on (a) XuNet and (b) SiaStegNet.

(IIS, AIS) exhibit a significant performance drop under these degradations. This superior performance highlights the robustness of MIDAS to channel noise and attack, which is a critical advantage of our diffusion-based approach.

More Experiments. Additional evaluations on a different dataset and a high-capacity scenario ($N = 8$), together with ablation studies on the key algorithmic components of MIDAS, different model checkpoints, and hyperparameters, are provided in Appendices C and D, respectively. These results demonstrate the robustness and scalability of MIDAS across datasets, extreme-capacity settings, and model checkpoints, while validating the effectiveness of our core strategies and modules and characterizing the impact of individual hyperparameters.

5. Conclusion

This paper presents MIDAS, a training-free framework for access-controlled CIS utilizing pre-trained diffusion models. By leveraging the Random Basis and Latent Vector Fusion, MIDAS achieves robust access control and high-fidelity reconstruction without the need for resource-intensive training. Extensive experiments confirm that MIDAS outperforms training-free CIS baselines in both security and access control. Owing to its superior access control, MIDAS facilitates flexible and efficient communication in various multi-user scenarios through private key distribution based on information access privileges. However, as the diffusion process can involve inference latency, optimizing sampling strategies for improved efficiency could be a meaningful extension.

Impact Statement

In this work, we propose MIDAS, a training-free and access-controlled scheme for coverless image steganography using pre-trained diffusion models. This capability makes our approach highly effective for implementing robust access control in practical communication scenarios that preclude resource-intensive training. By enabling selective and secure data sharing, even scalable given its multi-image hiding capability, our algorithm holds the potential to enhance the privacy and practical utility of coverless image steganography systems in real-world applications. However, as this technology could be exploited for privacy attacks, such as unauthorized data exfiltration, its ethical implications warrant careful attention within communities where stego-images are shared.

References

- Agustsson, E. and Timofte, R. Ntire 2017 challenge on single image super-resolution: Dataset and study. In *Proceedings of the IEEE Conference on Computer Vision and Pattern Recognition (CVPR) Workshops*, pp. 126–135, 2017.
- Akl, S. G. and Taylor, P. D. Cryptographic solution to a problem of access control in a hierarchy. *ACM Transactions on Computer Systems*, 1(3):239–248, 1983.
- Baluja, S. Hiding images in plain sight: Deep steganography. In *Advances in Neural Information Processing Systems*, volume 30, 2017.
- Bharatwaj, A. K. and Hasabnis, A. R. Steganography in the quantum era. In *2024 International Conference on Emerging Smart Computing and Informatics (ESCI)*, pp. 1–5, 2024.
- Chan, C.-K. and Cheng, L. Hiding data in images by simple lsb substitution. *Pattern Recognition*, 37(3):469–474, 2004.
- Chen, L., Feng, B., Xia, Z., Lu, W., and Weng, J. Robust generative steganography for image hiding using concatenated mappings. *IEEE Transactions on Information Forensics and Security*, 2025.
- Greenberg, O., Kishon, E., and Lischinski, D. Seed-to-seed: Unpaired image translation in diffusion seed space. In *36th British Machine Vision Conference*, 2025.
- Guan, Z., Jing, J., Deng, X., Xu, M., Jiang, L., Zhang, Z., and Li, Y. Deepmih: Deep invertible network for multiple image hiding. *IEEE Transactions on Pattern Analysis and Machine Intelligence*, 45(1):372–390, 2022.
- Guo, J., Tian, B., Jiang, J., and Dong, L. Enabling diverse styles coverless image steganography with two-stage latent transformation and diffusion model. *Journal of Information Security and Applications*, 97:104328, 2026.
- Gurunath, R., Klaib, M. F. J., Samanta, D., and Khan, M. Z. Social media and steganography: use, risks and current status. *IEEE Access*, 9:153656–153665, 2021.
- Issac, B. M., Kumar, S., Zafar, S., Shakil, K. A., and Wani, M. A. Deep learning steganography for big data security using squeeze and excitation with inception architectures. *Scientific Reports*, 15(1):31193, 2025.
- Jafari, R., Ziou, D., and Rashidi, M. M. Increasing image compression rate using steganography. *Expert Systems with Applications*, 40(17):6918–6927, 2013.
- Jing, J., Deng, X., Xu, M., Wang, J., and Guan, Z. Hinet: Deep image hiding by invertible network. In *Proceedings of the IEEE/CVF International Conference on Computer Vision (ICCV)*, pp. 4733–4742, 2021.
- Kweon, H., Park, J., Woo, S., and Cho, D. Deep multi-image steganography with private keys. *Electronics*, 10(16), 2021.
- Liao, X., Yin, J., Guo, S., Li, X., and Sangaiah, A. K. Medical jpeg image steganography based on preserving inter-block dependencies. *Computers and Electrical Engineering*, 67:320–329, 2018.
- LiChen, B., Shao, S., zikai zhou, Qi, Z., zhiqiang xu, Xiong, H., and Xie, Z. Zigzag diffusion sampling: Diffusion models can self-improve via self-reflection. In *The Thirteenth International Conference on Learning Representations*, 2025.
- Lu, S.-P., Wang, R., Zhong, T., and Rosin, P. L. Large-capacity image steganography based on invertible neural networks. In *Proceedings of the IEEE/CVF Conference on Computer Vision and Pattern Recognition (CVPR)*, pp. 10816–10825, 2021.
- Mali, S. N., Patil, P. M., and Jalnekar, R. M. Robust and secured image-adaptive data hiding. *Digital Signal Processing*, 22(2):314–323, 2012.
- Qin, T., Feng, B., Zhou, B., Zhang, J., Xia, Z., Weng, J., and Lu, W. Jpeg compression-resistant generative image hiding utilizing cascaded invertible networks. *IEEE Transactions on Information Forensics and Security*, 20: 6019–6032, 2025.
- Radford, A., Kim, J. W., Hallacy, C., Ramesh, A., Goh, G., Agarwal, S., Sastry, G., Askell, A., Mishkin, P., Clark, J., Krueger, G., and Sutskever, I. Learning transferable visual models from natural language supervision. In

- Proceedings of the 38th International Conference on Machine Learning*, volume 139, pp. 8748–8763, 2021.
- Rombach, R., Blattmann, A., Lorenz, D., Esser, P., and Ommer, B. High-resolution image synthesis with latent diffusion models. In *Proceedings of the IEEE/CVF Conference on Computer Vision and Pattern Recognition (CVPR)*, pp. 10684–10695, 2022.
- Simmons, G. J. The prisoners’ problem and the subliminal channel. In *Advances in cryptology: proceedings of crypto 83*, pp. 51–67, 1984.
- Song, J., Meng, C., and Ermon, S. Denoising diffusion implicit models. In *International Conference on Learning Representations*, 2021.
- Wallace, B., Gokul, A., and Naik, N. Edict: Exact diffusion inversion via coupled transformations. In *Proceedings of the IEEE/CVF Conference on Computer Vision and Pattern Recognition (CVPR)*, pp. 22532–22541, 2023.
- Wang, Z., Bovik, A., Sheikh, H., and Simoncelli, E. Image quality assessment: from error visibility to structural similarity. *IEEE Transactions on Image Processing*, 13(4):600–612, 2004.
- Xu, G., Wu, H.-Z., and Shi, Y.-Q. Structural design of convolutional neural networks for steganalysis. *IEEE Signal Processing Letters*, 23(5):708–712, 2016.
- Xu, Y., Mou, C., Hu, Y., Xie, J., and Zhang, J. Robust invertible image steganography. In *Proceedings of the IEEE/CVF Conference on Computer Vision and Pattern Recognition (CVPR)*, pp. 7875–7884, 2022.
- Xu, Y., Zhang, X., Yu, J., Mou, C., Meng, X., and Zhang, J. Diffusion-based hierarchical image steganography. *arXiv preprint arXiv:2405.11523*, 2024.
- Yang, S., Wu, T., Shi, S., Lao, S., Gong, Y., Cao, M., Wang, J., and Yang, Y. Maniqa: Multi-dimension attention network for no-reference image quality assessment. In *Proceedings of the IEEE/CVF Conference on Computer Vision and Pattern Recognition (CVPR) Workshops*, pp. 1191–1200, 2022.
- Yang, Y., Liu, Z., Jia, J., Gao, Z., Li, Y., Sun, W., Liu, X., and Zhai, G. Diffstega: Towards universal training-free coverless image steganography with diffusion models. In *Proceedings of the Thirty-Third International Joint Conference on Artificial Intelligence*, pp. 1579–1587, 2024.
- You, W., Zhang, H., and Zhao, X. A siamese cnn for image steganalysis. *IEEE Transactions on Information Forensics and Security*, 16:291–306, 2021.
- Yu, J., Zhang, X., Xu, Y., and Zhang, J. Cross: Diffusion model makes controllable, robust and secure image steganography. In *Advances in Neural Information Processing Systems*, volume 36, pp. 80730–80743, 2023.
- Zhang, L., Rao, A., and Agrawala, M. Adding conditional control to text-to-image diffusion models. In *Proceedings of the IEEE/CVF International Conference on Computer Vision (ICCV)*, pp. 3836–3847, 2023.
- Zhang, R., Isola, P., Efros, A. A., Shechtman, E., and Wang, O. The unreasonable effectiveness of deep features as a perceptual metric. In *Proceedings of the IEEE Conference on Computer Vision and Pattern Recognition (CVPR)*, 2018.
- Zhou, J., Lu, Y., and Lu, G. Individualized image steganography method with dynamic separable key and adaptive redundancy anchor. *Knowledge-Based Systems*, 309: 112729, 2025a.
- Zhou, J., Lu, Y., Wen, J., and Lu, G. Efficient and separate authentication image steganography network. In *Forty-second International Conference on Machine Learning*, 2025b.

A. Architecture of MIDAS

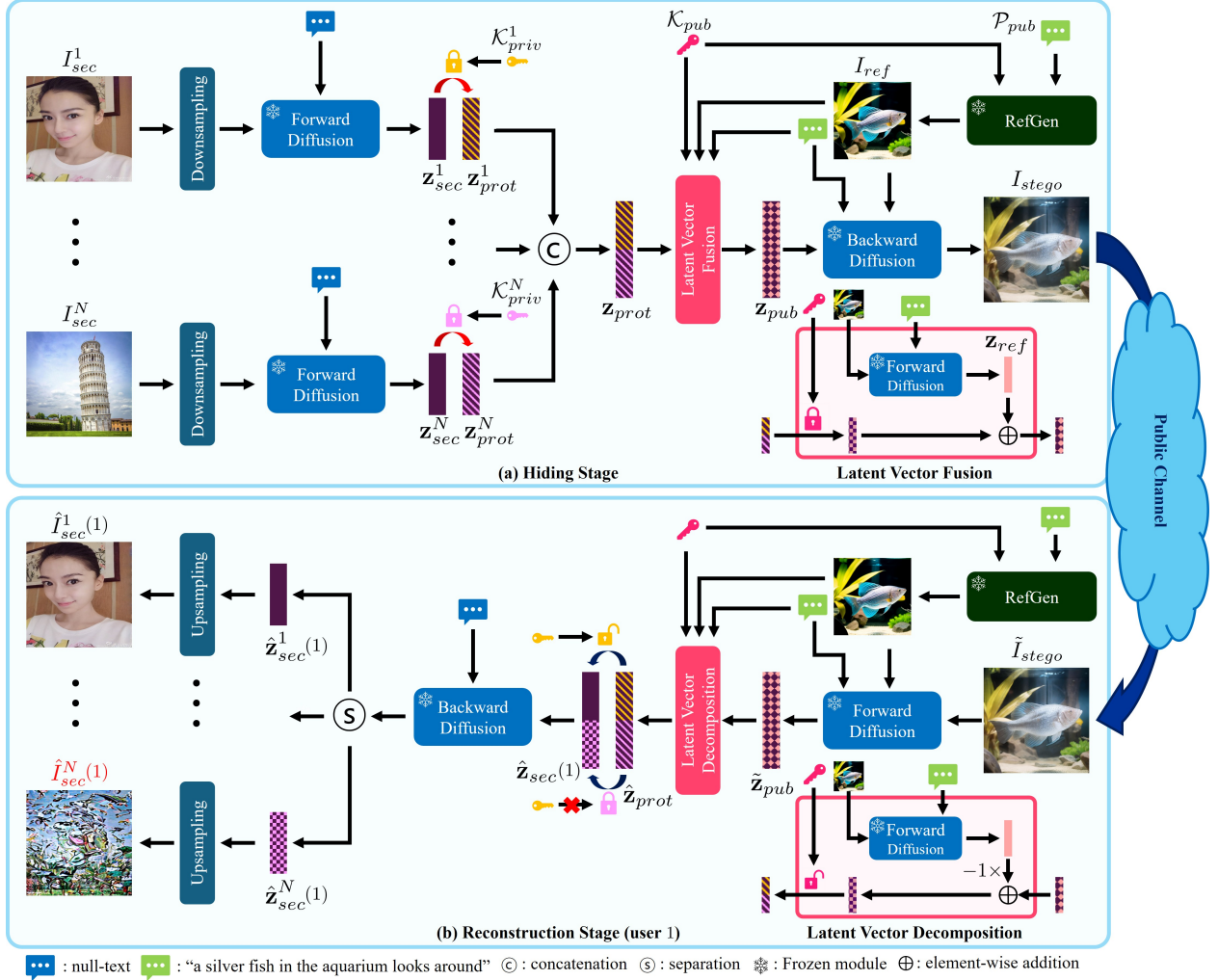


Figure 5. The overall architecture of MIDAS. (a) The Hiding Stage, where N secret images ($I_{sec}^1, \dots, I_{sec}^N$) are individually encrypted using private keys (\mathcal{K}_{priv}^i) and then jointly fused using the public key (\mathcal{K}_{pub}) to form the single stego image (I_{stego}). (b) The Reconstruction Stage (for user 1), where user 1 recovers their assigned image (\hat{I}_{sec}^1) using \mathcal{K}_{priv}^1 , from the received stego image (\tilde{I}_{stego}) (which may contain noise due to transmission errors), while the access control mechanism ensures that other images remain encrypted.

B. Experimental Details

B.1. Construction of Random Basis Matrix

To construct Q_d , an intermediate orthonormal matrix $Q'_{\lfloor \gamma d \rfloor} \in \mathbb{R}^{\lfloor \gamma d \rfloor \times \lfloor \gamma d \rfloor}$ is first generated via QR decomposition using a seed \mathcal{K} . This matrix is then extended into a larger block-diagonal form, $\text{diag}(Q'_{\lfloor \gamma d \rfloor}, I)$, where the remaining entries are filled by an identity matrix. Finally, Q_d is obtained by shuffling the rows of this block-diagonal matrix, with the permutation order determined by the same seed \mathcal{K} .

B.2. Implementation Details

All experiments were conducted in a Python 3.12.9 environment equipped with an AMD Ryzen Threadripper PRO 3955WX (16-core) processor and an NVIDIA RTX 3090 GPU. For the diffusion model, the total time step is set to $T = 50$ and the EDICT (Wallace et al., 2023) mixing coefficient to 0.93. To ensure high-quality reconstruction, only a portion ξ of the total steps is executed; the diffusion process thus runs over steps $[0, \xi T]$. We define the private diffusion stage as the phase where secret images are inverted, and the public diffusion stage as the phase where the fused latent is reconstructed into the stego image. We set $\xi = 0.4$ for the private diffusion stage and the Latent Vector Fusion stage (to get \mathbf{z}_{ref}), and $\xi = 0.7$ for the public diffusion stage. For $N > 1$, $\gamma_{priv} = 0.4$ and $\gamma_{fuse} = 0.5$ are used. For $N = 1$, since latent vector mixing is unnecessary, we set $\gamma_{fuse} = 0$ and $\gamma_{priv} = 0.5$. In the Latent Vector Fusion, $\alpha = 0.95$ is used. Furthermore, for $N > 1$, a 5-step DDIM (Song et al., 2021) forward process is applied immediately following Private Key Encryption, followed by a 5-step DDIM backward process prior to the User Access Control stage. We empirically found that this intermediate DDIM sequence significantly enhances reconstruction quality. The source code is available in the supplementary material.

To evaluate CRoSS* (Yu et al., 2023) and DiffStega* (Yang et al., 2024) in a multi-user environment, we extend their official implementations by incorporating the latent concatenation mechanism utilized in MIDAS. For all the other hyperparameters (e.g., diffusion steps and key strength), we follow the default settings provided in their respective original papers.

CRoSS*: For a set of secret images $\{I_{sec}^1, \dots, I_{sec}^N\}$, each image is independently processed via a DDIM forward pass using its specific private prompt. The resulting latent vectors are then concatenated and denoised using a public prompt to generate I_{stego} . In our implementation, we adopted separate denoising for each secret image, as this approach was found to yield superior results for this baseline.

DiffStega*: Each secret image $\{I_{sec}^1, \dots, I_{sec}^N\}$ undergoes an individual DDIM forward pass with a null-text prompt, followed by encryption using distinct private keys K_{priv} via the Noise Flip mechanism. These encrypted latents are concatenated, and an additional Noise Flip operation is applied to the combined vector. The final latent is denoised with a public prompt and a reference image to produce I_{stego} . The reconstruction is performed using a joint denoising strategy.

While the original DiffStega was optimized for single-image scenarios, we introduce DiffStega**, which adopts the same diffusion steps and key strengths as MIDAS to ensure a fair comparison (see Appendix D.3 for details).

DiffStega**: We set the private key strength to $\gamma_{priv} = 0.2$ and the public key strength to $\gamma_{fuse} = 0.25$, while also applying the same 5-step intermediate DDIM sequence used in MIDAS. Under these settings, the signal-to-noise ratio between the original and encrypted latents aligns with that of Random Basis encryption, ensuring an equitable comparison.

We utilize the source caption as the private prompt for CRoSS*, whereas DiffStega*, DiffStega** and MIDAS exclusively employ null-text prompts. For reconstruction under a wrong K_{priv} where $N > 1$, we evaluate each model by attempting decryption with the K_{priv} of every other authorized user. In the $N = 1$ case, where no other users exist, the protocols differ: CRoSS* is tested using a null-text prompt as the incorrect key, while the other training-free CIS models utilize a mismatched random seed.

For modification-based baselines, IIS (Zhou et al., 2025a) and AIS (Zhou et al., 2025b) were retrained using their official open-source implementations on the DIV2K dataset (Agustsson & Timofte, 2017).

For steganalysis, we randomly sample pairs of cover and stego images, splitting them into a training set (80%) and a validation set (20%). We employ XuNet (Xu et al., 2016) and SiaStegNet (You et al., 2021) using available open-source implementations.⁴ Both models are trained for 50 epochs, and the version achieving the highest validation accuracy is selected for evaluation.

⁴<https://github.com/albblgb/Deep-Steganalysis>

C. More Experiments

C.1. Qualitative Results of Hiding Four Images

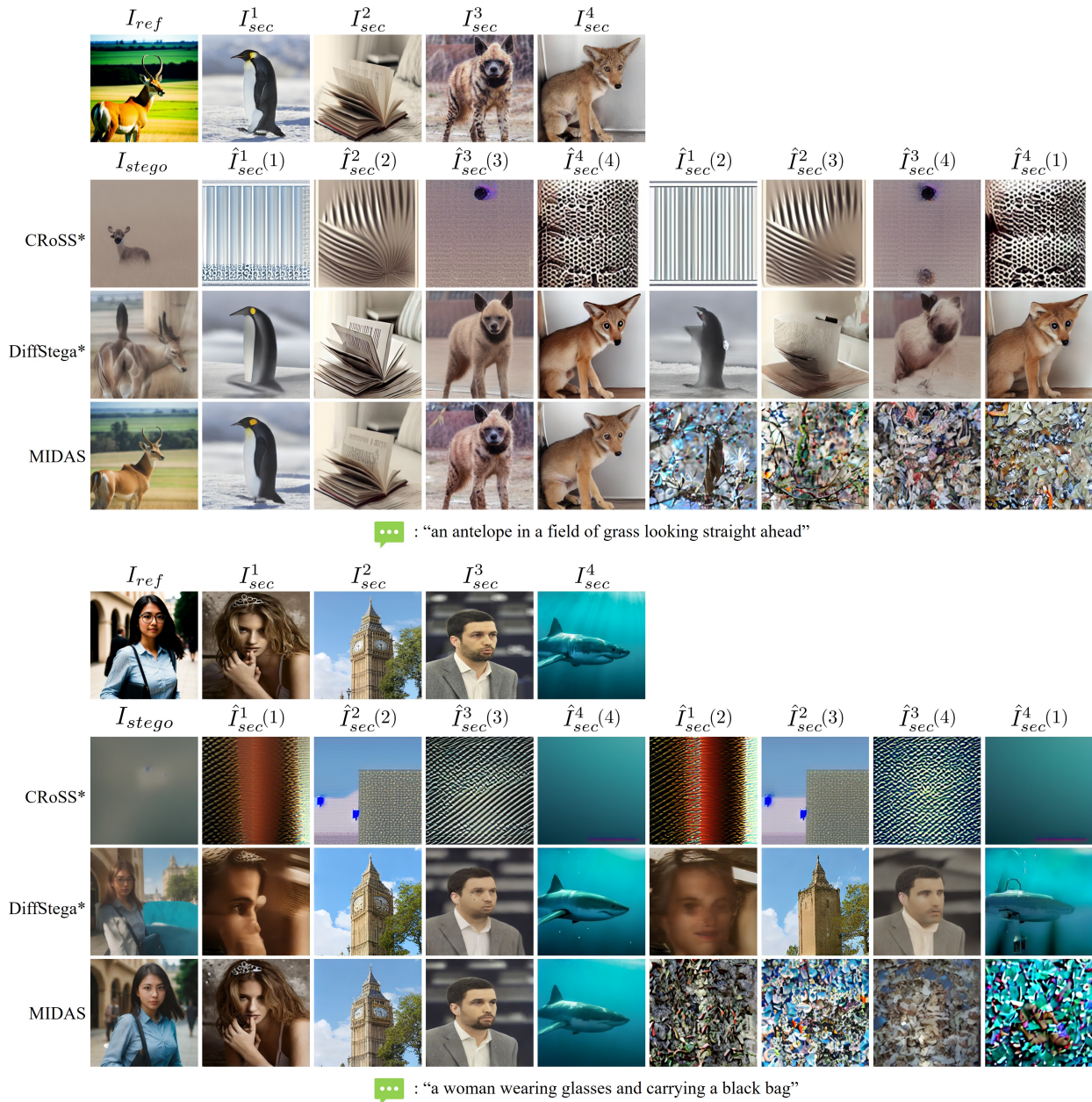


Figure 6. Visual comparisons of MIDAS, CRoSS*, and DiffStega* on the Stego260 dataset under different prompts for four-image hiding.

C.2. Experimental Results on UniStega

Table 4. Quantitative results for stego and reconstructed images on the UniStega dataset.

N	Method	Stego image quality	Stego image diversity				Correct \mathcal{K}_{priv} reconstruction			Wrong \mathcal{K}_{priv} reconstruction		
		MANIQA \uparrow	PSNR \downarrow	SSIM \downarrow	LPIPS \uparrow	CLIP Score \uparrow	PSNR \uparrow	SSIM \uparrow	LPIPS \downarrow	PSNR \downarrow	SSIM \downarrow	LPIPS \uparrow
1	IIS	-	-	-	-	-	42.724	0.995	0.032	10.497	0.125	0.786
	AIS	-	-	-	-	-	31.585	0.997	0.155	22.484	0.634	0.342
	CRoSS*	0.445	19.452	0.646	0.397	27.574	21.116	0.713	0.322	17.415	0.564	0.480
	DiffStega*	0.439	18.450	0.581	0.471	28.676	23.183	0.767	0.269	18.614	0.589	0.429
	MIDAS(Ours)	0.409	13.329	0.380	0.658	29.127	21.196	0.677	0.336	13.236	0.218	0.680
2	IIS	-	-	-	-	-	36.053	0.984	0.104	11.707	0.244	0.776
	AIS	-	-	-	-	-	28.651	0.973	0.302	4.573	0.098	0.856
	CRoSS*	0.442	15.336	0.468	0.597	25.912	17.196	0.519	0.524	15.469	0.446	0.584
	DiffStega*	0.413	16.380	0.459	0.592	27.550	20.638	0.654	0.393	17.471	0.519	0.498
	MIDAS(Ours)	0.458	10.431	0.254	0.760	29.974	22.563	0.701	0.346	10.104	0.092	0.751
4	IIS	-	-	-	-	-	30.819	0.959	0.215	14.910	0.348	0.666
	AIS	-	-	-	-	-	25.916	0.945	0.365	5.259	0.102	0.979
	CRoSS*	0.385	13.177	0.377	0.691	23.313	12.567	0.247	0.709	12.321	0.237	0.718
	DiffStega*	0.360	15.657	0.438	0.632	27.238	18.408	0.538	0.491	16.975	0.478	0.550
	MIDAS(Ours)	0.483	10.408	0.298	0.780	29.813	21.557	0.635	0.399	10.987	0.136	0.739

C.3. Very Large Capacity

Table 5. Quantitative results of MIDAS on stego and reconstructed images for eight-image hiding.

N	Dataset	Stego image quality	Stego image diversity				Correct \mathcal{K}_{priv} reconstruction			Wrong \mathcal{K}_{priv} reconstruction		
		MANIQA \uparrow	PSNR \downarrow	SSIM \downarrow	LPIPS \uparrow	CLIP Score \uparrow	PSNR \uparrow	SSIM \uparrow	LPIPS \downarrow	PSNR \downarrow	SSIM \downarrow	LPIPS \uparrow
8	Stego260	0.456	9.698	0.357	0.785	30.257	20.502	0.624	0.440	11.219	0.187	0.731
	UniStega	0.421	10.320	0.316	0.799	29.084	19.439	0.543	0.502	11.230	0.167	0.738



Figure 7. Qualitative results of MIDAS on the Stego260 dataset under different prompts for eight-image hiding.

D. Ablation Study

D.1. Effectiveness of Encryption Strategy.

As shown in prior work (LiChen et al., 2025), residual structural information in the latent vector can degrade the diffusion model’s generation quality when the structural information is poorly aligned with the generative prompt. Noise Flip, which only inverts the signs of the latent values, inherently preserves some spatial information from the original image. In contrast, Random Basis alters the latent vector by modifying the actual values, thereby more effectively scrambling and eliminating such spatial information.

To quantitatively verify this effect, we compare the amount of residual structural information remaining after applying Random Basis versus Noise Flip. We use an extremely high key strength to maximize the observable effect to the mechanisms. The evaluation protocol is as follows:

1. Apply DDIM forward diffusion to the original image.
2. Apply the key mechanism to K channels out of the four diffusion latent vector channels. Increasing K lowers the structural similarity between the pre- and post-encryption latent vectors.
3. Generate the encrypted image using DDIM backward diffusion on the encrypted vector.

We measure the structural similarity between the original image and the encrypted image in terms of the structural component (S) of SSIM defined as follows:

$$S(\mathbf{x}, \mathbf{y}) = \frac{2\sigma_{\mathbf{xy}} + C}{\sigma_{\mathbf{x}}^2 + \sigma_{\mathbf{y}}^2 + C} \quad (4)$$

where \mathbf{x} and \mathbf{y} are input image patches, $\sigma_{\mathbf{x}}^2$ and $\sigma_{\mathbf{y}}^2$ are the local variances, $\sigma_{\mathbf{xy}}^2$ is the local covariance, and C is a stabilization constant. Note that a lower value of S indicates a lower structural similarity. Table 6 shows that Random Basis consistently achieves lower structural similarity than Noise Flip, regardless of the number of encrypted channels.

Table 6. Quantification of residual structural information in the stego image, measured by the structural component of SSIM between I_{sec} and I_{stego} .

Method	Number of encrypted channels				
	0	1	2	3	4
Noise Flip	0.809	0.582	0.355	0.201	0.089
Random Basis	0.809	0.560	0.286	0.128	0.048

D.2. Effectiveness of Diffusion Strategy.

In the Reconstruction Stage of MIDAS, each user i employs joint denoising of the full latent vector $\hat{\mathbf{z}}_{sec}(i)$ instead of denoising the individual segments $\hat{\mathbf{z}}_{sec}^1(i), \dots, \hat{\mathbf{z}}_{sec}^N(i)$ separately. As shown in Table 7, this joint denoising approach significantly outperforms separate denoising during reconstruction, yielding a $\text{PSNR}_{\text{Correct}}$ gain of approximately 1 dB. The superior performance can be attributed to the fact that the Stable Diffusion model is optimized for the 512×512 latent-space resolution. Processing the full latent $\mathbf{z}_{sec}(i)$ thus better exploits the model’s inherent contextual understanding and global coherence, leading to significantly improved reconstruction quality.

Table 7. Performance analysis across different diffusion strategies. $\text{PSNR}_{\text{Correct}}$ denote the PSNR values between the original secret images and their reconstructions using the correct \mathcal{K}_{priv} .

Method	MANIQA \uparrow	CLIP Score \uparrow	$\text{PSNR}_{\text{Correct}}\uparrow$
separate denoising	0.434	30.129	22.928
joint noising	0.417	30.074	23.901
MIDAS(Ours)	0.434	30.129	23.903

In contrast, applying joint noising during the Hiding Stage does not yield any improvement in either stego image quality or reconstructed image quality compared to separate processing. Moreover, adopting this complex joint process introduces a

potential security risk by allowing information to mingle across encrypted latent segments associated with different users. Therefore, joint noising is intentionally omitted during the Hiding Stage.

D.3. Effectiveness of Latent Vector Fusion.

Since the original parameters of CRoSS* and DiffStega* were optimized for the $N = 1$ case, the performance gap between these baselines and MIDAS may partly stem from parameter differences. To eliminate this factor, we construct DiffStega** by adopting the fair key strengths and diffusion steps used in MIDAS. We further evaluate MIDAS_{NF}, a variant of MIDAS where the Random Basis mechanism is replaced with a Noise Flip, to verify its specific effectiveness. Of note, MIDAS_{NF} serves as an intermediate variant to bridge the gap between DiffStega** and MIDAS by incorporating a weighted interpolation with \mathbf{z}_{ref} into the DiffStega** framework. This setup allows us to disentangle the performance gains provided by the fusion architecture from those achieved by the Random Basis mechanism.

Table 8 presents the results of our ablation study. While optimizing the parameters of DiffStega* (yielding DiffStega**) markedly improves diversity (higher CLIP Score) and reconstruction quality, it leads to a substantial degradation in perceptual stego image quality, as evidenced by a sharp drop in MANIQA scores. The introduction of our Latent Vector Fusion architecture effectively mitigates this degradation, significantly restoring stego image quality in MIDAS_{NF}. Notably, this architectural improvement not only recovers visual fidelity but also further enhances diversity, while maintaining robust reconstruction performance. Finally, the incorporation of the Random Basis mechanism provides further refinement, achieving the highest visual fidelity and diversity among all variants. These results demonstrate that the Latent Vector Fusion architecture and its Random Basis mechanism are essential for achieving the superior performance of MIDAS.

Table 8. Effectiveness of Latent Vector Fusion. PSNR_{Correct} and PSNR_{Wrong} denote the PSNR values between the original secret images and their reconstructions using the correct and incorrect \mathcal{K}_{priv} , respectively.

Method	MANIQA \uparrow	CLIP Score \uparrow	PSNR _{Correct} \uparrow	PSNR _{Wrong} \downarrow
DiffStega*	0.399	26.952	21.908	18.137
DiffStega**	0.324	28.459	24.091	10.769
MIDAS _{NF}	0.380	29.631	23.616	10.566
MIDAS(Ours)	0.434	30.129	23.903	9.964

D.4. Effectiveness of α .

Fig. 8 shows the experimental results of MIDAS with varying α , the parameter in (2) that balances $M_D \mathbf{z}_{prot}$ and \mathbf{z}_{ref} . As α decreases (i.e., the influence of the reference image grows), stego image quality is improved, however, this comes at the cost of reduced reconstruction quality. This result demonstrates the trade-off between stego naturalness and reconstruction accuracy governed by α .

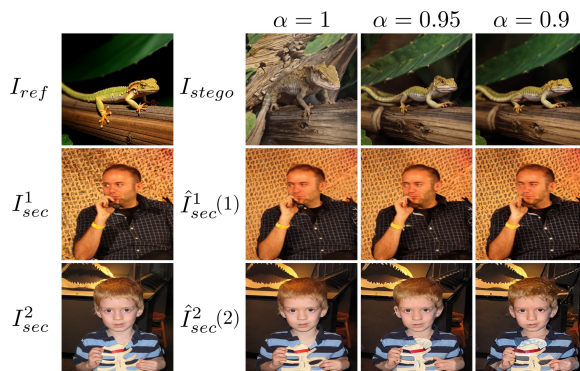


Figure 8. Experimental results of MIDAS with varying α .

D.5. Effectiveness of γ_{priv} and γ_{fuse} .

Fig. 9 illustrates the stego images generated by MIDAS with varying values of γ_{priv} and γ_{fuse} . Reconstructed images are omitted as their quality shows no significant change across these parameters. As shown in the figure, low values of γ_{priv} and γ_{fuse} result in poor stego quality, as the structural information of the secret images remains visible. However, as these parameters increase, the structural interference diminishes, yielding visually natural and high-quality stego images.

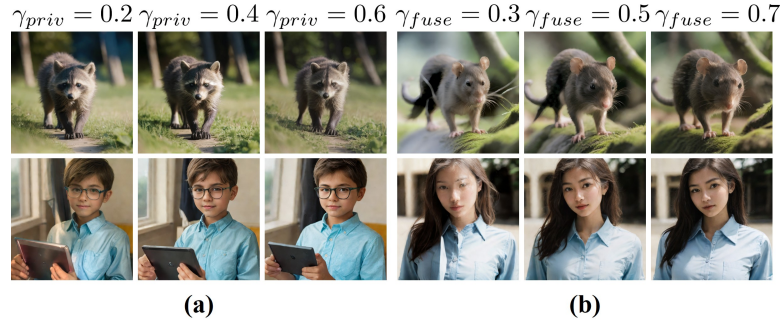


Figure 9. Visual comparisons of stego images generated by MIDAS with varying (a) γ_{priv} and (b) γ_{fuse} .

D.6. Effectiveness of Checkpoints.

Fig. 10 illustrates the experimental results of MIDAS with an alternative checkpoint while maintaining the same architecture.⁵ As shown in the figure, MIDAS consistently produces high-quality stego images and successful reconstructions across different checkpoints, demonstrating its strong generalizability.



Figure 10. Experimental results of MIDAS using an alternative checkpoint⁵.

⁵<https://huggingface.co/stablediffusionapi/majicmix-fantasy>